

Nanoscale

Accepted Manuscript



This is an *Accepted Manuscript*, which has been through the Royal Society of Chemistry peer review process and has been accepted for publication.

Accepted Manuscripts are published online shortly after acceptance, before technical editing, formatting and proof reading. Using this free service, authors can make their results available to the community, in citable form, before we publish the edited article. We will replace this *Accepted Manuscript* with the edited and formatted *Advance Article* as soon as it is available.

You can find more information about *Accepted Manuscripts* in the [Information for Authors](#).

Please note that technical editing may introduce minor changes to the text and/or graphics, which may alter content. The journal's standard [Terms & Conditions](#) and the [Ethical guidelines](#) still apply. In no event shall the Royal Society of Chemistry be held responsible for any errors or omissions in this *Accepted Manuscript* or any consequences arising from the use of any information it contains.



Nanoscale

ARTICLE

Growth of Nickel Silicate Nanoplates on Reduced Graphene Oxide as Layered Nanocomposite for Highly Reversible Lithium Storage

Received 00th January 20xx,
Accepted 00th January 20xx

DOI: 10.1039/x0xx00000x

www.rsc.org/

Qian-Qian Wang, Jin Qu*, Yuan Liu, Chen-Xi Gui, Shu-Meng Hao, Yunhua Yu and Zhong-Zhen Yu*

The combination of active materials with electrically conductive carbon materials and their contact efficiency are crucial for improving electrochemical performances of active materials. Here, nickel silicate (NiSiO_x) nanoplates are planted in situ on the surface of reduced graphene oxide (RGO) nanosheets to form a two dimensional face-to-face nanocomposite of NiSiO_x/RGO for lithium storage. Face-to-face structure enhances the contact efficiency of NiSiO_x with RGO, and thus leads to a higher reversible capacity and better rate performance of NiSiO_x/RGO nanocomposite than those of both carbon nanotube (CNT)@NiSiO_x nanocable and NiSiO_x. The layered NiSiO_x/RGO nanocomposite exhibits a high reversible specific capacity of 797 mA h/g, which is 62% and 806% higher than those of CNT@NiSiO_x nanocable and NiSiO_x alone, respectively.

Introduction

Lithium ion batteries (LIBs) are among the most important power sources for portable electronic devices such as mobile phones, laptops, pads and digital cameras¹⁻³ because of their long cycle life, high reversible capacity, high operating voltage, high energy density, and no memory effect.⁴⁻⁷ Nano-structured silicon and silicates have attracted lots of attention on many applications such as energy storage,⁸⁻¹¹ adsorption,¹²⁻¹⁵ molecular sieve¹⁶⁻¹⁸ and catalysts^{19, 20} due to their rich source, low cost, easy preparation, porous structure and environmentally benign. More importantly, the unique structure of layered silicates allows for the transfer of ions in the interlayer space and makes them possible candidates as anode materials for LIBs. However, the major disadvantage of metal silicates is their poor conductivity.²¹ Yang et al. synthesized Ni₃Si₂O₅(OH)₄ multi-walled nanotubes as anode materials for LIBs. The reduced nanotubes at 180 °C showed the first cycle discharge capacity of 1650 mA h/g and the discharge capacity of 308.5 mA h/g after 20 cycles at a low current density of 20 mA/g.²² Later, Yang et al. fabricated flower-like nickel oxide/nickel silicate nanocomposites as anode materials for LIBs, which exhibited the first cycle discharge capacity of 1440 mA h/g and the reversible capacity

of 126 mA h/g after 50 cycles at a current density of 20 mA/g.²³ The large irreversible capacities and fast capacity fading are probably due to the poor electrical conductivity of silicates and the large volume and structural change during the charge/discharge process. At present, there are few studies on silicate-based materials for LIBs, it is thus interesting to combine layered silicates with electrically conductive materials to improve their electrical conductivity and structural stability.

Electrically conductive carbon materials have been used to enhance electrochemical performances of active materials.^{2, 24-31} Zero-dimensional (0D) carbon nanoparticles were reported to construct an elastic and conductive shell to enhance cycle stability of Fe₃O₄ and Sn.^{32, 33} We introduced amorphous carbon into the interlayer and on the surface of zinc silicates by carbonizing glucose. The interlayer space could be tuned by varying the amount of carbon precursor, and the reversible specific capacity was increased by 96% from 232 mA h/g of zinc silicate to 455 mA h/g of zinc silicate with intercalated carbon.²¹ One-dimensional (1D) carbon nanotubes (CNT) or nanofibers also served as conductive cable to enhance reversible capacity and structure stability of Fe₂O₃, Sn and SnO_x.³⁴⁻³⁷ We reported CNT@layered nickel silicate (CNT@NiSiO_x) coaxial nanocables with a reversible specific capacity of 489 mA h/g at a current density of 50 mA/g, which is much higher than that of nickel silicate nanotube.³⁸ The dimensionality is crucial to the contact efficiency of active materials with carbon materials. Considering the two-dimensional (2D) feature of layered silicates,^{13, 39-42} 2D conductive material is preferred to form a face-to-face contact. Ions and electrons could be easily and quickly transferred between the two components, leading to high reversible capacity and excellent rate performance. In

State Key Laboratory of Organic-Inorganic Composites, College of Materials Science and Engineering, Beijing University of Chemical Technology, Beijing 100029, China. Fax: +86-10-64428582; E-mail: qujin@mail.buct.edu.cn (J. Qu), yuzz@mail.buct.edu.cn (Z.-Z. Yu)

Electronic Supplementary Information (ESI) available: XRD pattern, SEM and TEM images of GO; HRTEM image of NiSiO_x/RGO after 50 cycles, charge capacities of NiSiO_x/RGO nanocomposites. Electrochemical impedance spectra of NiSiO_x, NiSiO_x/RGO, and CNT@NiSiO_x. See DOI: 10.1039/x0xx00000x

contrast, the face-to-point contact between 2D layered silicates and 0D amorphous carbon nanoparticle shell (or conductive carbon black) and the face-to-line contact between 2D layered silicates and 1D carbon nanotube (or nanofiber) may degrade the intrinsic capability of layered silicates.

Graphene has become a potential electrode material due to its high specific surface area, large surface-to-volume ratio, excellent electrical conductivity, good chemical properties and excellent flexibility.⁴³⁻⁴⁶ It is worth mentioning that lithium ions can be stored on the edges, defects, and disorders of graphene sheets.⁴⁷ Many researchers focused on combining graphene with metal oxide based materials to improve the electrochemical performance of LIBs.⁴⁸⁻⁵² We reported a face-to-face α -Fe₂O₃/reduced graphene oxide (RGO) nanocomposite by oxygen bridges, exhibiting a high reversible capacity and excellent rate performance than α -Fe₂O₃ alone.⁵³ It is really an efficient way to combine 2D layered silicate with graphene for improving their electrical conductivity, reversible capacity and cycling performance of LIBs.

Herein, a face-to-face structure of layered nickel silicate (NiSiOx)/RGO is designed to grow NiSiOx nanoplates on RGO using a mild hydrothermal process. Both NiSiOx and RGO serve as hosts for lithium ions. NiSiOx nanoplates are well distributed onto RGO nanosheets to prevent the restacking of RGO, while RGO acts as a soft matrix to support the volume change resulted from the intercalation/deintercalation of lithium ions during the charge/discharge process. Moreover, the high conductivity of RGO reduces the interfacial resistance and improves the specific capacity. The resulting NiSiOx/RGO nanocomposite exhibits an excellent cycling performance with a high reversible specific capacity of 797 mA h/g after 50 cycles, and it also shows good rate performances at various current densities. The reversible capacity of NiSiOx/RGO nanocomposite is 1.6 times that of CNT@NiSiOx at the same current density.³⁸ The better electrochemical performance of the 2D fact-to-face structure than the face-to-line structure reveals the importance of nanocomposite design for LIB anodes.

Experimental section

Materials

Graphite was purchased from Huadong Graphite Factory (China) with an average diameter of 13 μ m. Sulfuric acid (H₂SO₄, 98%), hydrochloric acid (HCl, 37%), hydrogen peroxide (H₂O₂), ammonium hydroxide (NH₃·H₂O, 28%), nickel chloride (NiCl₂·6H₂O), ammonia chloride (NH₄Cl) and tetraethyl orthosilicate (TEOS) were bought from Beijing Chemical Factory (Beijing, China). Amorphous fumed silica was provided by Alfa Aesar China Co., Ltd. All chemicals are of analytical grade and were used without further purification.

Synthesis of NiSiOx/RGO layered nanocomposite

Graphite oxide was prepared by a modified Hummers method and silica/RGO was fabricated using a reported approach.¹⁵ NiSiOx/RGO nanocomposite was then prepared by a

hydrothermal process: 50 mg silica/RGO was dispersed in 20 mL deionized water by ultrasonication as suspension A; 178.3 mg nickel chloride, 530.5 mg ammonia chloride and 1 mL ammonium hydroxide were dissolved in 30 mL deionized water as solution B. Suspension A and solution B were mixed and the mixture was transferred to an autoclave and maintained at 90 °C for 10 h. The resulting product was collected by centrifugation, washed with deionized water for several times, and dried in an oven at 60 °C for 12 h. For comparison, graphene oxide (GO) was treated with a similar hydrothermal method to get RGO. Layered NiSiOx was also synthesized with amorphous fumed silica, instead of silica/RGO, under the same condition.

Characterization

NiSiOx/RGO nanocomposite, RGO and NiSiOx were characterized with a Thermo VG RSCAKAB 250X high resolution X-ray photoelectron spectroscopy (XPS), a Nicolet Nexus 670 Fourier-transform infrared spectroscopy (FT-IR) and a Renishaw Via Raman microscopy (Britain). X-ray diffraction (XRD) measurement was carried out with a Rigaku D/Max 2500 diffractometer with Cu K α radiation (λ =1.54 Å) at a generator voltage of 40 kV and a generator current of 40 mA. The morphology and microstructure of the nanocomposite were observed with a Zeiss Supra 55 field-emission scanning electron microscope (SEM) and a JEOL JEM-3010 transmission electron microscope (TEM). Thermogravimetric analysis (TGA) measurements were conducted using a TA Instruments Q50 thermogravimetric analyzer at a heating rate of 10 °C/min in air atmosphere.

Electrochemical Measurements

Electrochemical performances of NiSiOx/RGO nanocomposite, NiSiOx and RGO were evaluated using coin-type cells assembled in an argon-filled glove box. The working electrode consisting of 70 wt% active material (NiSiOx/RGO, NiSiOx or RGO), 20 wt% super-P as conductive agent, and 10 wt% poly(vinylidene fluoride) was fabricated by casting the slurry onto a Ni foam. The size of the circular electrode discs is 14 mm in diameter, and the mass loading is approximately 1.0 mg/cm². The coin cells were assembled using lithium foil as the counter electrode, mesoporous polyethylene/polypropylene membrane as the separator, and the electrolyte was 1 M LiPF₆ dissolved in a mixture of ethylene carbonate, dimethyl carbonate, and diethyl carbonate with a mass ratio of 1:1:1 (Tianjin Jinniu Power Source Materials Co., Ltd.). Cyclic voltammograms (CV) and electrochemical impedance spectroscopy (EIS) were recorded on a Metrohm Autolab PGSTAT 302N electrochemical workstation. CV measurements were conducted at a scanning rate of 0.1 mV/s within the voltage range of 0.01-3.0 V. For EIS measurement, the AC modulation amplitude is 10 mV and the applied frequency range is from 10 kHz to 0.1 Hz. The cycling performance and rate capacity of the assembled cells were carried out on Land CT 2001A electrochemical workstation at the current densities of 50-1000 mA/g and the voltage range from 0.01 to 3.0 V (vs. Li⁺/Li).

Results and discussion

NiSiOx/RGO nanocomposite is synthesized by a two-step approach using silica as the hard template and the intermediate product. Firstly, TEOS hydrolyzes in the presence of ammonium hydroxide and generates silica on the surface of GO nanosheets by connecting with the functional groups of GO. Secondly, by adding ammonium hydroxide and ammonium chloride to adjust the pH value of the suspension, silica gradually dissolves and reacts with nickel ions to form NiSiOx nanosheets that are covalently bonded onto GO during the hydrothermal treatment at a fairly mild temperature below the boiling point of water. Simultaneously, GO is reduced to RGO, which exhibits a better electrical conductivity than GO, and NiSiOx/RGO nanocomposite is thus obtained.

Figure 1a shows the XRD patterns of NiSiOx and NiSiOx/RGO nanocomposite. All the peaks at 19.4° , 24.6° , 35.9° and 60.7° can be indexed to $\text{Ni}_3\text{Si}_2\text{O}_5(\text{OH})_4$ (JCPDS No. 20-0791), with no impurities observed. Neat GO exhibits a sharp peak at around 12° (Figure S1), and it shows a smooth surface with micron scale lateral size (Figures S2 and S3). The hydrolysis of TEOS in the presence of GO leads to the formation of numerous silica nanoparticles that are homogeneously distributed on GO (Figure 1b). By the hydrothermal treatment, NiSiOx nanoplates are formed in situ from silica nanoparticles and decorated tightly on RGO nanosheet (Figure 1c). Such nanoplates efficiently prevent the restacking of RGO nanosheets and maintain a high specific surface area of NiSiOx/RGO nanocomposite. Furthermore, RGO nanosheets buffer the volume change and keep the structure of the nanocomposite stable during the charge/discharge process. The homogeneous distribution of the NiSiOx nanoplates is also observed (Figure 1d), and their lamellar structure with an average interlayer spacing of 0.75 nm is clearly revealed in Figure 1e, which agrees well with the crystal structure information of NiSiOx (Figure 1f). Such a large interlayer space would benefit the intercalation/deintercalation of lithium ions and thus improve lithium ions storage performance.

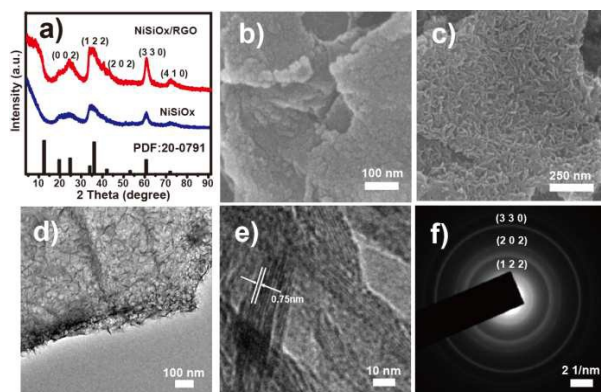


Figure 1. a) XRD patterns of NiSiOx and NiSiOx/RGO; SEM images of b) SiO_2/RGO and c) NiSiOx/RGO; d) TEM and e) HRTEM images, and f) selected area electron diffraction pattern of NiSiOx/RGO.

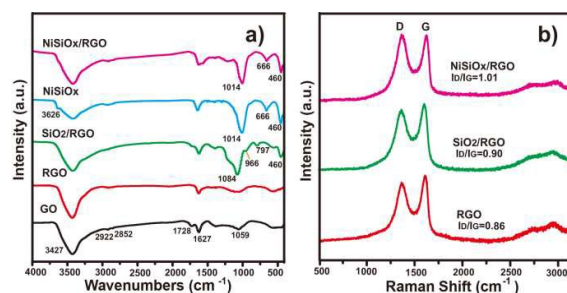


Figure 2. a) FT-IR spectra of GO, RGO, SiO_2/RGO , NiSiOx and NiSiOx/RGO; b) Raman spectra of RGO, SiO_2/RGO and NiSiOx/RGO.

To reflect the structural and composition changes of the nanocomposites, Figure 2a shows FT-IR spectra of GO, RGO, SiO_2/RGO , NiSiOx and NiSiOx/RGO. For GO, the peak at 3427 cm^{-1} is attributed to the stretching vibration of -OH, or caused by adsorbed water. The peak at 1728 cm^{-1} corresponds to C=O stretching vibration in the ketone/carboxyl groups, and the peaks of GO and RGO at 1627 cm^{-1} relate to the C=C stretching vibration.⁵⁴⁻⁵⁷ For SiO_2/RGO , the strong and broad adsorption peak at 1084 cm^{-1} is associated with the anti-symmetric stretching vibration of Si-O-Si, and the peaks at 966 and 797 cm^{-1} correspond to the stretching vibration of Si-OH and the symmetric Si-O-Si network stretching vibration, respectively. The peak at 460 cm^{-1} is attributed to the symmetric stretching vibration of Si-O.⁵⁸⁻⁶¹ These peaks demonstrate the formation of silica network on RGO nanosheets during the sol-gel process.^{15,57} After the hydrothermal treatment, a new peak at 1014 cm^{-1} can be identified as the formation of Si-O-Ni bond, and that at 666 cm^{-1} corresponds to the vibration of Ni-O in NiSiOx.⁵⁸ A new peak at 3626 cm^{-1} is attributed to the vibration of Ni-OH.⁶²⁻⁶⁴ Similar peaks are also observed in NiSiOx/RGO, confirming the successful formation of NiSiOx/RGO nanocomposite.

To investigate the structural change during the preparation process, Figure 2b shows Raman spectra of RGO, SiO_2/RGO and NiSiOx/RGO nanocomposites. For carbon based material, D band at 1340 cm^{-1} is related to the structure defects, while G band at 1590 cm^{-1} is associated with the first-order scattering of the E_{2g} mode of sp^2 carbon domains. I_D/I_G ratio is widely used as a representative of the graphitization degree of carbon materials.⁶⁵ The I_D/I_G ratio increases from 0.86 for RGO to 0.9 for SiO_2/RGO , and further to 1.01 for NiSiOx/RGO, indicating the destruction of carbon domains due to the combination of NiSiOx with RGO and suggesting that the structural defects are introduced to RGO nanosheets after the hydrothermal process. These defects and disorders could provide more storage sites for lithium ions.^{66,67}

Based on TGA results of NiSiOx/RGO nanocomposite and NiSiOx (Figure 3a), the content of NiSiOx is $\sim 79.4\text{ wt}\%$ in NiSiOx/RGO and it is stable in a wide temperature range. The mass loss may result from the loss of hydrated water in the silicate layers. XPS is used to study the composition change of the nanocomposites before and after the hydrothermal process. The presence of carbon, oxygen, silicon, nickel elements are proved by XPS survey scan spectra of GO,

SiO₂/RGO, NiSiOx and NiSiOx/RGO (Figure 3b). Reduction of GO is reflected in its C 1s XPS spectra (Figure 3c). The peak at 286.5 eV corresponds to epoxide/ether group, which decreases obviously from GO to NiSiOx/RGO, indicating the gradual reduction of GO to RGO during the preparation process.^{15, 57} In the Si 2p XPS spectra (Figure 3d), the peaks at 102.1, 103.0 and 103.9 eV are related to Ni-O₃-Si, C-O₃-Si and O-Si-O, respectively. The presence of C-O₃-Si bond in SiO₂/RGO and NiSiOx/RGO indicates the formation of silica network and the covalent bonding between GO and silica.^{15, 38, 57} Compared to SiO₂/RGO, O-Si-O bond decreases in NiSiOx/RGO and Ni-O₃-Si bond increases, confirming the conversion of SiO₂ to NiSiOx. The results of FI-IR, Raman, XRD and XPS spectra along with TEM observation confirm the successful formation of NiSiOx/RGO nanocomposite.

Figure 4 shows the electrochemical behavior of RGO, NiSiOx and NiSiOx/RGO. The first cycle discharge capacities of NiSiOx (Figure 4a) and RGO (Figure 4b) are 835 and 1296 mA h/g and the reversible capacities after 50 cycles decrease to 88 and 480 mA h/g, respectively. Thus, the charge capacity retentions of NiSiOx and RGO are as low as 20 % and 65 %, respectively. Interestingly, the first cycle discharge capacity of NiSiOx/RGO is 1237 mA h/g (Figure 4c), 48% higher than that of NiSiOx and similar to that of RGO. Its reversible capacity is still retained at 797 mA h/g after 50 cycles, nearly the same as the first charge capacity. Such a high reversible capacity is 9 times that of NiSiOx, and 66 % higher than that of RGO. Because RGO content is just 20.6 wt%, the reversible capacity of the nanocomposite should mainly result from NiSiOx component. It is confirmed that the enhanced reversible capacity is higher than reported in literature on silicate based nanomaterials for LIBs (Table 1).^{21-23, 38, 68-70}

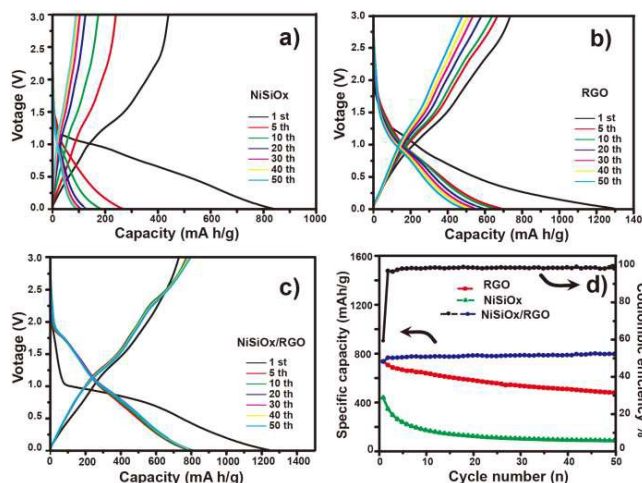


Figure 4. The charge/discharge curves of a) NiSiOx, b) RGO and c) NiSiOx/RGO for 1st, 5th, 10th, 20th, 30th, 40th and 50th cycle at a current density of 50 mA/g; d) cycling performances of NiSiOx/RGO, NiSiOx and RGO at the current density of 50 mA/g, and Coulombic efficiency of NiSiOx/RGO within a voltage window of 0.01-3.0 V (vs. Li⁺/Li).

The first cycle Columbic efficiency of NiSiOx/RGO is 59.4 % (Figure 4d), which is due to the irreversible process of forming SEI film. The formation of SEI film is a double-edged sword. On one hand, it consumes the lithium ions and leads to a large irreversible specific capacity in the first charge/discharge cycle; on the other hand, it forms a protecting layer on the surface of electrode material and prevents further consumption of the material. The charge and discharge capacities of both NiSiOx and RGO fall off quickly with the charge/discharge cycles, while the charge capacity of NiSiOx/RGO maintains highly stable with all charge/discharge curves almost overlay with each other except for the first cycle, revealing excellent cycle stability and high lithium ions storage capacity of NiSiOx/RGO during the lithium ion intercalation/deintercalation process. Importantly, the sheet-on-sheet structure of NiSiOx/RGO still retains after the 50 charge/discharge cycles (Figure S4). Such excellent structure stability would benefit the electrochemical performance of NiSiOx/RGO and thus improves its cycle stability and rate performance.

Table 1. Specific capacities of silicate nanostructures in literatures.

| Samples | Morphology | Current density (mA/g) | 50 th charge capacity (mA h/g) | Ref. |
|---|-------------|------------------------|---|-----------|
| Ni ₃ Si ₂ O ₅ (OH) ₄ | nanotube | 20 | 309 ^a | 22 |
| Ni ₃ Si ₂ O ₅ (OH) ₄ /NiO | nanoflower | 20 | 126 | 23 |
| NiSNT | hollow tube | 50 | 107 | 38 |
| CNT@NiSiOx | nanocable | 50 | 489 | 38 |
| ZnSiC | nanoflower | 50 | 162 | 21 |
| Zn ₂ SiO ₄ | nanorod | 50 | 388 ^b | 68 |
| Zn ₂ SiO ₄ | microsphere | 50 | 413 ^b | 69 |
| RGO/NiSiO/Ni | sandwich | 20 | 524 ^c | 70 |
| NiSiOx/RGO | nanosheet | 50 | 797 | This work |

^a: the capacity of 21th cycle; ^b: the capacity of 20th cycle; ^c: the capacity of 55th cycle

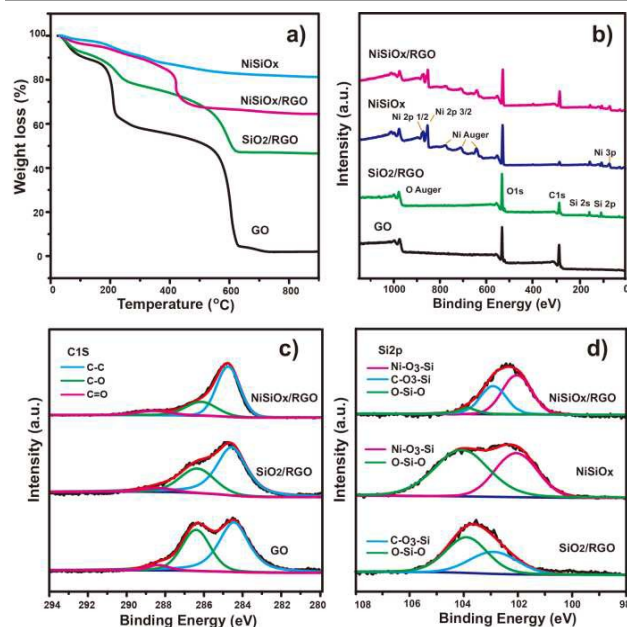


Figure 3. a) TG curves and b) survey scans spectra of GO, SiO₂/RGO, NiSiOx and NiSiOx/RGO; c) C 1s XPS spectra of GO, SiO₂/RGO and NiSiOx/RGO; d) Si 2p XPS spectra of SiO₂/RGO, NiSiOx and NiSiOx/RGO.

In the CV curves, the broad peak at around 0.50 V for both NiSiOx (Figure 5a) and NiSiOx/RGO (Figure 5b) corresponds to the formation of SEI film; and it diminishes and almost disappears in subsequent cycles, proving the SEI film formation is an irreversible process. In the second cycle, new peaks appeared at 1.56 V for NiSiOx and NiSiOx/RGO may be due to the insertion of lithium ions into NiSiOx nanoplates and thus the formation of $\text{Li}_x\text{Ni}_3\text{Si}_2\text{O}_5(\text{OH})_4$.²² The second and third cycle CV curves of NiSiOx are slightly different while those of NiSiOx/RGO are almost the same, confirming the excellent electrochemical reaction reversibility. Figure 5c shows the reversible charge capacities of NiSiOx/RGO, NiSiOx and RGO at various rates of 50-1000 mA/g. NiSiOx/RGO exhibits superior rate performance than NiSiOx and RGO. The reversible specific capacities of NiSiOx/RGO at current densities of 100, 200 and 500 mA/g are 656, 601 and 534 mA h/g, respectively. Even at the current density of 1000 mA/g, the reversible specific capacity of NiSiOx/RGO is still retained at 484 mA h/g, which is 2.3 times that of RGO. However, there is nearly no capacity observed for NiSiOx alone. When the current density returns to 50 mA/g after all cycles, the reversible capacity of NiSiOx/RGO reaches 787 mA h/g, even higher than the initial specific capacity, which may be owing to the activation of the electrode material after the cycles.⁷¹⁻⁷³ After the rate performance test (60 cycles), we proceed its long cycling rate performance test at current densities of 500, 1000, 2000 and 4000 mA/g for 200 cycles in total, and the reversible specific capacities of NiSiOx/RGO are 640, 570, 432 and 301 mA h/g, respectively (Figure S5). The results indicate that even after 260 cycles at various densities, NiSiOx/RGO nanocomposite still retains excellent reversible specific capacity and cycling stability. Figure 5d shows EIS curves of NiSiOx/RGO and NiSiOx, which show semicircle shapes in the high frequency region and inclined lines in the low frequency region. The diameter of the semicircle is related to the SEI film resistance and the electron transfer resistance of the electrode/electrolyte interface. The slope of the inclined line represents the diffusion resistance of lithium ions in the electrode material. NiSiOx/RGO shows a smaller semicircle diameter than neat NiSiOx and reported CNT@NiSiOx, meaning a lower charge transfer resistance; NiSiOx/RGO also reveals the highest slope value of the inclined line, represents a faster lithium ion diffusion rate and smaller variation of diffusion path (Figure S6).^{74,75}

All these results demonstrate the synergistic effect of NiSiOx and RGO. RGO is used to construct a conductive network and acts as the supporting matrix for NiSiOx. Compared to reported face-to-line or face-to-point modes, the face-to-face structure with higher contact efficiency effectively improves the electrical conductivity of the nanocomposite and thus benefits the fast mass transfer of electron and lithium ions between RGO and NiSiOx. The first cycle discharge specific capacity of NiSiOx/RGO is ~ 1.2 times that of CNT@NiSiOx, and even after 50 cycles at the current density of 50 mA/g, the reversible capacity of the former is 1.6 times that of the latter. The 2D face-to-face structure makes NiSiOx and RGO exhibit a large contact surface area and thus more effectively connects NiSiOx and RGO with each other to construct a shorter lithium

ions diffusion path between them than 1D face-to-line structure, which improves the transfer performance of electrons and lithium ions in NiSiOx/RGO nanocomposite. In addition, the larger interlayer space of RGO than that of MWCNT is more beneficial for the intercalation of lithium ions and more suitable as the buffer to sustain the volume and structural change during the charge/discharge cycles. Therefore, NiSiOx/RGO nanocomposite exhibits not only a better cycling stability performance but also an enhanced rate performance than CNT@NiSiOx. The reversible specific capacity of NiSiOx/RGO nanocomposite at a current density of 1000 mA/g is also 210% higher than that of CNT@NiSiOx nanocable, which again confirms the advantage of 2D face-to-face NiSiOx/RGO nanocomposite in enhancing the fast diffusion and transfer of electrons and lithium ions to get a better electrochemical performance.

In summary, the reasons for the good lithium ions storage performance of NiSiOx/RGO nanocomposite, especially its excellent cycling and rate performance, are as follows: First, the face-to-face structure of NiSiOx/RGO enlarges the effective contact surface area and shortens the diffusion routes of electrons and lithium ions, which is in favor of the improvement of lithium ion storage performance. Second, RGO provides a conductive network to improve the electrical conductivity of the nanocomposite and contribute to a fast transfer of electrons and ions. Third, RGO acts as the supporting material for NiSiOx to sustain the volume and structural change during the intercalation/deintercalation process and thus enhance the structural stability during the charge/discharge process. In addition to the main active material of NiSiOx, RGO provides additional active site to store lithium ions for increasing the specific capacity of the nanocomposite.

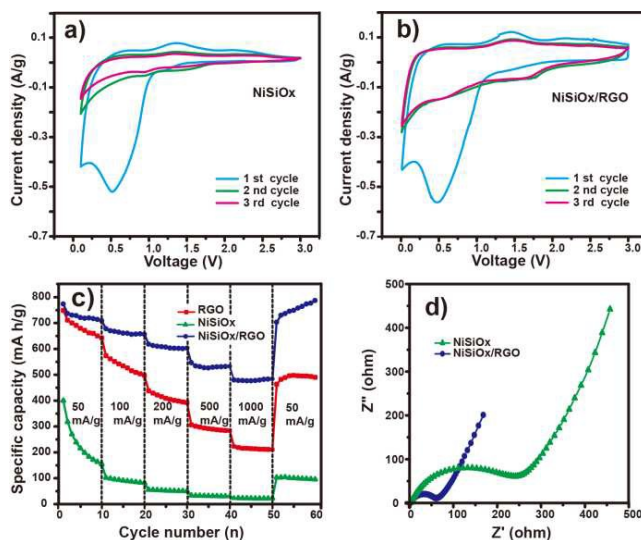


Figure 5. The cyclic voltammograms curves of a) NiSiOx and b) NiSiOx/RGO for 1st, 2nd, 3rd cycle at a scan rate of 0.1 mVs⁻¹ from 0.01 to 3.0 V; c) reversible charge capacities of NiSiOx/RGO, NiSiOx and RGO at various rates of 50-1000 mA/g; d) Nyquist plots of the NiSiOx/RGO and NiSiOx.

Conclusion

Layered nanocomposite of NiSiO_x/RGO with covalent bonding between NiSiO_x and RGO is prepared by growth of NiSiO_x nanoplates onto RGO nanosheets using a mild hydrothermal method. NiSiO_x nanoplates are well dispersed on RGO nanosheets in a face-to-face manner to prevent the restacking of RGO, while RGO provides a conductive network to improve the electrical conductivity and acts as a matrix to sustain the volume change during the intercalation/deintercalation of lithium ions. Moreover, NiSiO_x/RGO nanocomposite exhibits a synergistic effect between NiSiO_x and RGO for lithium ions storage performance. The 2D face-to-face structure of NiSiO_x/RGO increases effective contact area between active materials and electrolyte, shortens the diffusion pathway of lithium ions, and facilitates electrons and lithium ions transfer, leading to higher reversible specific capacity, excellent cycling stability and better rate performance than those of NiSiO_x and RGO. Even after 50 cycles, the reversible capacity of NiSiO_x/RGO nanocomposite is as high as 797 mA h/g, ~9 times that of NiSiO_x and 66 % higher than that of RGO. All the results indicate that constructing a 2D face-to-face structure with conductive materials is an effective approach to improve the electrochemical properties of 2D energy storage materials, such as sodium storage and supercapacitor.

Acknowledgements

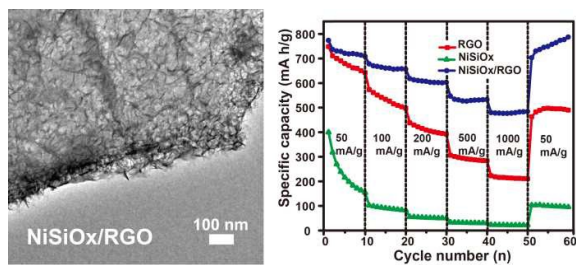
Financial support from the National Natural Science Foundation of China (51402012, 51125010), the Fundamental Research Funds for the Central Universities (YS201402), and the State Key Laboratory of Organic-Inorganic Composites (201404) is gratefully acknowledged.

Notes and references

- Chen, J.; Cheng, F., *Acc. Chem. Res.* **2009**, *42*, 713-723.
- Liang, M. H.; Zhi, L. J., *J. Mater. Chem.* **2009**, *19*, 5871-5878.
- Tarascon, J. M.; Armand, M., *Nature* **2001**, *414*, 359-367.
- Liu, C.; Li, F.; Ma, L. P.; Cheng, H. M., *Adv. Mater.* **2010**, *22*, E28-E62.
- Armand, M.; Tarascon, J. M., *Nature* **2008**, *451*, 652-657.
- Goodenough, J. B.; Park, K. S., *J. Am. Chem. Soc.* **2013**, *135*, 1167-1176.
- Manthiram, A., *J. Phys. Chem. Lett.* **2011**, *2*, 176-184.
- Wu, H.; Cui, Y., *Nano Today* **2012**, *7*, 414-429.
- Wu, H.; Zheng, G.; Liu, N.; Carney, T. J.; Yang, Y.; Cui, Y., *Nano Lett.* **2012**, *12*, 904-909.
- Choi, N. S.; Yao, Y.; Cui, Y.; Cho, J., *J. Mater. Chem.* **2011**, *21*, 9825-9840.
- Chan, C. K.; Patel, R. N.; O'Connell, M. J.; Korgel, B. A.; Cui, Y., *ACS Nano* **2010**, *4*, 1443-1450.
- Ide, Y.; Ochi, N.; Ogawa, M., *Angew. Chem. Int. Ed.* **2011**, *50*, 654-656.
- Yang, Y.; Zhuang, Y.; He, Y. H.; Bai, B.; Wang, X., *Nano Res.* **2010**, *3*, 581-593.
- Qu, J.; Li, W.; Cao, C. Y.; Yin, X. J.; Zhao, L.; Bai, J.; Qin, Z.; Song, W. G., *J. Mater. Chem.* **2012**, *22*, 17222-17226.
- Gui, C. X.; Wang, Q. Q.; Hao, S. M.; Qu, J.; Huang, P. P.; Cao, C. Y.; Song, W. G.; Yu, Z. Z., *ACS Appl. Mater. Interfaces* **2014**, *6*, 14653-14659.
- Selvam, P.; Bhatia, S. K.; Sonwane, C. G., *Ind. Eng. Chem. Res.* **2001**, *40*, 3237-3261.
- Reddy, K. M.; Moudrakovski, I.; Sayari, A., *J. Chem. Soc., Chem. Commun.* **1994**, *9*, 1059-1060.
- Kuznicki, S. M.; Bell, V. A.; Nair, S.; Hillhouse, H. W.; Jacobinas, R. M.; Braunbarth, C. M.; Toby, B. H.; Tsapatsis, M., *Nature* **2001**, *412*, 720-724.
- Park, J. C.; Lee, H. J.; Bang, J. U.; Park, K. H.; Song, H., *Chem. Commun.* **2009**, *47*, 7345-7347.
- Fang, Q. L.; Xuan, S. H.; Jiang, W. Q.; Gong, X. L., *Adv. Funct. Mater.* **2011**, *21*, 1902-1909.
- Qu, J.; Yan, Y.; Yin, Y. X.; Guo, Y. G.; Song, W. G., *ACS Appl. Mater. Interfaces* **2013**, *5*, 5777-5782.
- Yang, Y.; Liang, Q. Q.; Li, J. H.; Zhuang, Y.; He, Y. H.; Bai, B.; Wang, X., *Nano Res.* **2011**, *4*, 882-890.
- Yang, Y.; Jin, R. X.; Song, S. Y.; Xing, Y., *Mater. Lett.* **2013**, *93*, 5-8.
- Yan, J.; Fan, Z. J.; Sun, W.; Ning, G. Q.; Wei, T.; Zhang, Q.; Zhang, R. F.; Zhi, L. J.; Wei, F., *Adv. Funct. Mater.* **2012**, *22*, 2632-2641.
- Fan, Z. J.; Yan, J.; Wei, T.; Zhi, L. J.; Ning, G. Q.; Li, T. Y.; Wei, F., *Adv. Funct. Mater.* **2011**, *21*, 2366-2375.
- Zhou, J. S.; Song, H. H.; Chen, X. H.; Zhi, L. J.; Yang, S. B.; Huo, J. P.; Yang, W. T., *Chem. Mater.* **2009**, *21*, 2935-2940.
- Cui, G.; Hu, Y. S.; Zhi, L.; Wu, D.; Lieberwirth, I.; Maier, J.; Mullen, K., *Small* **2007**, *3*, 2066-2069.
- Zhai, D. Y.; Li, B. H.; Du, H. D.; Gao, G. Y.; Gan, L.; He, Y. B.; Yang, Q. H.; Kang, F. Y., *Carbon* **2012**, *50*, 5034-5043.
- Luo, B.; Fang, Y.; Wang, B.; Zhou, J. S.; Song, H. H.; Zhi, L. J., *Energy Environ. Sci.* **2012**, *5*, 5226-5230.
- Zhu, X. J.; Zhu, Y. W.; Murali, S.; Stollers, M. D.; Ruoff, R. S., *ACS Nano* **2011**, *5*, 3333-3338.
- Wang, D.; Choi, D.; Li, J.; Yang, Z.; Nie, Z.; Kou, R.; Hu, D.; Wang, C.; Saraf, L. V.; Zhang, J.; Aksay, I. A.; Liu, J., *ACS Nano* **2009**, *3*, 907-914.
- Zhang, W. M.; Wu, X. L.; Hu, J. S.; Guo, Y. G.; Wan, L. J., *Adv. Funct. Mater.* **2008**, *18*, 3941-3946.
- Zhang, W. M.; Hu, J. S.; Guo, Y. G.; Zheng, S. F.; Zhong, L. S.; Song, W. G.; Wan, L. J., *Adv. Mater.* **2008**, *20*, 1160-1165.
- Chi, C.; Lan, J. L.; Sun, J. M.; Liu, Y.; Yu, Y. H.; Yang, X. P., *RSC Adv.* **2015**, *5*, 41210-41217.
- Cho, J. S.; Hong, Y. J.; Kang, Y. C., *ACS Nano* **2015**, *9*, 4026-4035.
- Yu, Y. H.; Yang, Q.; Teng, D. H.; Yang, X. P.; Ryu, S. K., *Electrochem. Commun.* **2010**, *12*, 1187-1190.
- Liu, Y.; Yan, X. D.; Lan, J. L.; Teng, D. H.; Yu, Y. H.; Yang, X. P., *Electrochim. Acta* **2014**, *137*, 9-16.
- Gui, C. X.; Hao, S. M.; Liu, Y.; Qu, J.; Yang, C.; Yu, Y. H.; Wang, Q. Q.; Yu, Z. Z., *J. Mater. Chem. A* **2015**, *3*, 16551-16559.
- Zhuang, Y.; Yang, Y.; Xiang, G. L.; Wang, X., *J. Phys. Chem. C* **2009**, *113*, 10441-10445.
- Ray, S. S.; Maiti, P.; Okamoto, M.; Yamada, K.; Ueda, K., *Macromolecules* **2002**, *35*, 3104-3110.
- Sinha Ray, S.; Okamoto, M., *Prog. Polym. Sci.* **2003**, *28*, 1539-1641.
- Pavlidou, S.; Papaspyrides, C. D., *Prog. Polym. Sci.* **2008**, *33*, 1119-1198.
- Park, S.; Ruoff, R. S., *Nature Nanotech.* **2009**, *4*, 217-224.
- Novoselov, K. S.; Geim, A. K.; Morozov, S. V.; Jiang, D.; Zhang, Y.; Dubonos, S. V.; Grigorieva, I. V.; Firsov, A. A., *Science* **2004**, *306*, 666-669.
- Geim, A. K., *Science* **2009**, *324*, 1530-1534.
- Lv, W.; Tang, D. M.; He, Y. B.; You, C. H.; Shi, Z. Q.; Chen, X. C.; Chen, C. M.; Hou, P. X.; Liu, C.; Yang, Q. H., *ACS Nano* **2009**, *3*, 3730-3736.
- Ji, L. W.; Lin, Z.; Alcoutlabi, M.; Zhang, X. W., *Energy Environ. Sci.* **2011**, *4*, 2682-2699.

- 48 Mai, Y. J.; Wang, X. L.; Xiang, J. Y.; Qiao, Y. Q.; Zhang, D.; Gu, C. D.; Tu, J. P., *Electrochim. Acta* **2011**, *56*, 2306-2311.
- 49 Wu, Z. S.; Ren, W. C.; Wen, L.; Gao, L. B.; Zhao, J. P.; Chen, Z. P.; Zhou, G. M.; Li, F.; Cheng, H. M., *ACS Nano* **2010**, *4*, 3187-3194.
- 50 Chang, K.; Chen, W. X., *Chem. Commun.* **2011**, *47*, 4252-4254.
- 51 Ding, S.; Luan, D.; Boey, F. Y.; Chen, J. S.; Lou, X. W., *Chem. Commun.* **2011**, *47*, 7155-7157.
- 52 Wang, B.; Wu, X. L.; Shu, C. Y.; Guo, Y. G.; Wang, C. R., *J. Mater. Chem.* **2010**, *20*, 10661-10664.
- 53 Qu, J.; Yin, Y. X.; Wang, Y. Q.; Yan, Y.; Guo, Y. G.; Song, W. G., *ACS Appl. Mater. Interfaces* **2013**, *5*, 3932-3936.
- 54 Zhang, Y.; Liu, H.; Zhu, Z. H.; Wong, K. w.; Mi, R.; Mei, J.; Lau, W. m., *Electrochim. Acta* **2013**, *108*, 465-471.
- 55 Wu, X. Z.; Zhou, J.; Xing, W.; Wang, G. Q.; Cui, H. Y.; Zhuo, S. P.; Xue, Q. Z.; Yan, Z. F.; Qiao, S. Z., *J. Mater. Chem.* **2012**, *22*, 23186-23193.
- 56 Li, X.; Hu, Y.; Liu, J.; Lushington, A.; Li, R.; Sun, X., *Nanoscale* **2013**, *5*, 12607-12615.
- 57 Hsiao, M. C.; Ma, C. C.; Chiang, J. C.; Ho, K. K.; Chou, T. Y.; Xie, X.; Tsai, C. H.; Chang, L. H.; Hsieh, C. K., *Nanoscale* **2013**, *5*, 5863-5871.
- 58 Wu, Y.; Chang, G.; Zhao, Y.; Zhang, Y., *Dalton Trans.* **2014**, *43*, 779-783.
- 59 Zhang, S. W.; Xu, W. Q.; Zeng, M. Y.; Li, J.; Li, J. X.; Xu, J. Z.; Wang, X. K., *J. Mater. Chem. A* **2013**, *1*, 11691-11697.
- 60 Wan, C.; Chen, B., *Nanoscale* **2011**, *3*, 693-700.
- 61 Ali, I. M.; Kotp, Y. H.; El-Naggar, I. M., *Desalination* **2010**, *259*, 228-234.
- 62 Li, H. B.; Yu, M. H.; Wang, F. X.; Liu, P.; Liang, Y.; Xiao, J.; Wang, C. X.; Tong, Y. X.; Yang, G. W., *Nat Commun.* **2013**, *4*, 1894.
- 63 Zhang, J. L.; Liu, H. D.; Shi, P.; Li, Y. J.; Huang, L. H.; Mai, W. J.; Tan, S. Z.; Cai, X., *J. Power Sources* **2014**, *267*, 356-365.
- 64 Liu, H. D.; Zhang, J. L.; Zhang, B.; Shi, L.; Tan, S. Z.; Huang, L. H., *Electrochim. Acta* **2014**, *138*, 69-78.
- 65 Stankovich, S.; Dikin, D. A.; Piner, R. D.; Kohlhaas, K. A.; Kleinhammes, A.; Jia, Y.Y.; Wu, Y.; Nguyen, S. T.; Ruoff, R. S., *Carbon*, **2007**, *45*, 1558-1565.
- 66 Zou, Y.; Wang, Y., *Nanoscale* **2011**, *3*, 2615-2620.
- 67 Zhou, X. Y.; Zou, Y. L.; Yang, J., *J. Power Sources* **2014**, *253*, 287-293.
- 68 Zhang, S. Y.; Lu, M.; Li, Y.; Sun, F.; Yang, J. C.; Wang, S. L., *Mater. Lett.* **2013**, *100*, 89-92.
- 69 Zhang, S. Y.; Ren, L.; Peng, S. J., *CrystEngComm* **2014**, *16*, 6195-6202.
- 70 Jin, R.; Yang, Y.; Li, Y.; Liu, X.; Xing, Y.; Song, S.; Shi, Z., *Chem.-Eur. J.* **2015**, *21*, 9014-9017.
- 71 Wang, Z. Y.; Luan, D. Y.; Madhavi, S.; Hu, Y.; Lou, X. W., *Energy Environ. Sci.* **2012**, *5*, 5252-5256.
- 72 Zeng, Z. P.; Zhao, H. L.; Lv, P. P.; Zhang, Z. J.; Wang, J.; Xia, Q., *J. Power Sources* **2015**, *274*, 1091-1099.
- 73 Zhu, J. X.; Yin, Z. Y.; Yang, D.; Sun, T.; Yu, H.; Hoster, H. E.; Hng, H. H.; Zhang, H.; Yan, Q. Y., *Energy Environ. Sci.* **2013**, *6*, 987-993.
- 74 Wen, W.; Wu, J. M.; Jiang, Y. Z.; Yu, S. L.; Bai, J. Q.; Cao, M. H.; Cui, J., *Sci Rep* **2015**, *5*, 11804.
- 75 Wu, H.; Xu, M.; Wang, Y. C.; Zheng, G. F., *Nano Res.* **2013**, *6*, 167-173.

TOC



The synthesized two dimensional face-to-face nanocomposite of Nickel silicate (NiSiOx)/reduced graphene oxide (RGO) for lithium storage exhibits a high reversible specific capacity of 797 mA h/g, 806% higher than that of NiSiOx.